International Journal of Disaster Risk Reduction 132 (2026) 105955

Contents lists available at ScienceDirect

International Journal of Disaster Risk Reduction

journal homepage: www.elsevier.com/locate/ijdrr

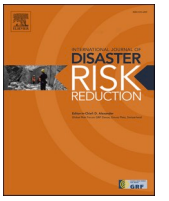

Portfolio-scale seismic fragility of RC bridge columns with series-distributed neural networks

Hoang Vinh Nguyen [a], Hoang Nam Phan [a,*], Duy Hoa Pham [b], Gianluca Quinci [c], Fabrizio Paolacci [c]

[a] Faculty of Road and Bridge Engineering, University of Science and Technology, The University of Danang, Da Nang, 550000, Viet Nam
[b] Faculty of Bridges and Roads, Hanoi University of Civil Engineering, Hanoi, 100000, Viet Nam
[c] Department of Civil, Computer Science and Aeronautical Technologies Engineering, Roma Tre University, 00146, Rome, Italy

ARTICLE INFO

Keywords:
Fragility curve
Rapid seismic vulnerability assessment
RC bridge column
Series distributed ANN
Surrogate model

ABSTRACT

This paper proposes a novel series-distributed artificial neural network framework for rapidly constructing seismic fragility curves of reinforced-concrete (RC) bridge columns at markedly reduced computational cost. Three coupled surrogate models are trained on datasets generated from nonlinear time-history and pushover analyses of RC piers with randomly sampled geometric and material properties subjected to hazard-consistent ground motions. The first network learns correlations among a reduced set of efficient ground-motion intensity measures (IMs), the second predicts drift demand from IMs and modelling parameters, and the third provides drift capacities for multiple damage states directly from capacity-curve information, thereby incorporating epistemic uncertainty in structural capacity. The trained surrogates are embedded in a Monte Carlo simulation scheme to estimate, in a largely non-parametric manner, the probability that drift demand exceeds capacity at each IM level. A case study on a portfolio of simply supported bridges in the Da Nang area, including selected bridges along National Highway 1A, demonstrates that the framework reproduces benchmark fragility curves from nonlinear analyses while achieving substantial reductions in analysis time. The results highlight systematic differences between rectangular and circular piers and quantify the impact of relaxing internal lognormal assumptions relative to traditional cloud-based fragility derivation. The proposed approach is implementation-ready, which relies on standard structural and ground-motion descriptors, delivers conventional fragility parameters, and is readily scalable to portfolio- and network-level seismic risk assessments and screening.

1. Introduction

Performance-based earthquake engineering provides the foundation for risk-informed decision-making in infrastructure networks [1]. For bridges, fragility curves quantify the probability of exceeding damage states as a function of ground-motion intensity and underpin portfolio-scale disaster risk reduction (DRR) decisions such as screening, prioritization, and planning [2]. Conventional procedures, such as cloud analysis [3], incremental dynamic analysis (IDA) [4], and multiple-stripe analysis (MSA) [5], are rigorous but computationally intensive and often depend on distributional assumptions that may not hold across heterogeneous inventories [6].

* Corresponding author.
E-mail address: phnam@dut.udn.vn (H.N. Phan).

https://doi.org/10.1016/j.ijdrr.2025.105955
Received 22 September 2025; Received in revised form 6 December 2025; Accepted 6 December 2025
Available online 7 December 2025

This limits timely application at the regional scale and constrains their utility for practice.

Researchers have continually advanced methodologies for developing fragility curves for bridge structures. Numerous studies have refined traditional techniques such as cloud analysis [7], IDA [8], and MSA [9], as well as proposed hybrid approaches that integrate elements of these methods to enhance the accuracy of probabilistic response modeling and damage state classification [6]. Recent research has also underscored the critical influence of uncertainties in structural modeling parameters and seismic hazard characteristics on the reliability of fragility assessments [8,10].

Although these simulation-based methods offer valuable insights into seismic vulnerability, they are often computationally demanding, particularly when applied to large-scale or geometrically complex structures with high-dimensional parameter spaces. This computational burden is further exacerbated when multiple ground motion scenarios must be considered to capture the full range of seismic demand. Several recent studies have highlighted these challenges, emphasizing the substantial time and resources required for high-fidelity nonlinear analyses and advocating for more efficient surrogate modeling techniques to reduce computational costs without compromising accuracy [11].

A DRR perspective extends beyond initial damage to include functionality, downtime, and recovery trajectories. Portfolio managers need tools that translate fragility into actionable indicators (e.g., probability of loss of service, screening-level risk indices) to support key priorities of the Sendai framework for disaster risk reduction on understanding risk and investing in resilience. This motivates efficient surrogate models that (i) scale to regional inventories, (ii) accommodate epistemic uncertainty in both demand and capacity, and (iii) produce outputs that integrate directly into agency workflows for screening and prioritization [12].

In response to the challenges associated with traditional simulation-based methods, machine learning (ML) techniques have gained significant momentum in earthquake engineering, offering efficient and scalable alternatives for seismic response prediction and fragility analysis [13–19]. A growing body of research has demonstrated the effectiveness of ML-based surrogate models in reducing computational demands while maintaining high accuracy in fragility assessments (see, for example, Ding et al. on regional building-portfolio fragility using a probabilistic ML approach with a Poisson binomial model) [18]. For instance, Mangalathu and Jeon [9] utilized a random-forest surrogate model to efficiently derive fragility curves for a multi-span reinforced-concrete (RC) bridge, significantly reducing analysis time. Among various ML techniques, artificial neural networks (ANNs) have emerged as particularly powerful tools for capturing complex, nonlinear relationships between seismic IMs and structural demands or damage states.

Several studies have integrated ANNs with traditional seismic analysis techniques to enhance fragility modeling. For example, Liu et al. [15] employed a hybrid framework combining ANNs with incremental dynamic analysis (IDA) to develop probabilistic response models, while Razzaghi et al. [16] used ANNs in conjunction with nonlinear dynamic simulations to construct fragility curves for RC bridges. An early contribution by Pang et al. [20] demonstrated that well-trained ANN models could serve as reliable surrogates for computationally intensive IDA procedures, while effectively accounting for uncertainties in material properties and geometric configurations. More recently, Liu et al. [21] proposed a knowledge-enhanced neural network for calibrating parameters in lumped plasticity models, combining physics-informed learning with data-driven techniques to enable accurate and rapid regional-scale seismic assessments. Parisi et al. [22] implemented ML algorithms for the cloud-based fragility analysis of existing multi-span simply supported girder bridges with a novel strategy to optimize the choice of input features. Beyond fragility modeling, ANNs and other ML algorithms have been applied in broader seismic applications such as damage detection, system identification, and structural health monitoring. Karakostas et al. [23] provided a comprehensive review of computational intelligence methods in this domain, emphasizing the utility of ML for understanding system responses under seismic excitation. Furthermore, a recent review by Marano et al. [24] highlighted the growing potential of deep learning architectures, including generative adversarial networks and recurrent neural networks, in generating synthetic seismic data and supporting advanced AI-driven evaluations of structural systems. Collectively, these contributions underscore the versatility, adaptability, and efficiency of ML, particularly ANN-based models, in addressing longstanding challenges in seismic vulnerability analysis and resilience-informed design, making them highly attractive tools for both researchers and practitioners in earthquake engineering.

While ML-based models facilitate rapid seismic fragility assessments by incorporating random input parameters, such as concrete compressive strength, steel yield strength, and pier geometry, they often retain a significant limitation: the reliance on the assumption that structural responses and IMs follow a specific probability distribution, often lognormal. This statistical simplification may not adequately capture the true variability and complexity of real-world seismic behavior. Moreover, a critical but often underrepresented issue in vulnerability assessments is the randomness of structural capacity, which is strongly influenced by epistemic uncertainty in structural parameters.

The seismic capacity of bridges is particularly sensitive to epistemic uncertainties stemming from limited or imprecise knowledge of material properties, geometric dimensions, and construction details, especially in aging or poorly documented infrastructure. Unlike aleatory variability, which is inherent and irreducible, epistemic uncertainty arises from incomplete information and can significantly affect the reliability of performance predictions. Numerous studies have emphasized the implications of disregarding epistemic uncertainty, which may result in substantial under- or overestimation of seismic vulnerability. For instance, Monteiro et al. [25] advocated for statistically characterizing both seismic capacity and demand through random sampling to effectively capture the influence of epistemic uncertainty on failure probabilities.

Similarly, Mangalathu et al. [26] demonstrated that seismic demand and fragility metrics are highly sensitive to a range of uncertain input parameters and proposed regression-based sensitivity analysis as a practical tool for quantifying their influence. At the regional level, Nettis et al. [27] showed that epistemic uncertainties in structural parameters can markedly alter loss estimation outcomes and impact prioritization strategies for bridge retrofitting and maintenance. Furthermore, Herrera et al. [28] revealed that incorporating epistemic uncertainty into reliability models leads to a significant increase in predicted failure probabilities, reinforcing the necessity of probabilistic frameworks that explicitly integrate such uncertainties to support seismic risk-informed decision-making.

Collectively, these studies highlight the essential role of incorporating epistemic uncertainty in seismic capacity modeling, leading to more robust, realistic, and defensible evaluations of bridge performance under earthquake loading, particularly in complex infrastructure networks where deterministic or overly simplified models risk overlooking critical vulnerabilities.

Accordingly, the present study proposes a novel series distributed ANN framework for the rapid seismic fragility assessment of a portfolio of bridge columns, designed to overcome the limitations of traditional methods by eliminating the need for the assumption of specific probabilistic distribution functions on IMs and structural responses. The framework comprises three interdependent ANN models trained on data generated from nonlinear static pushover and dynamic time-history analyses of a representative simply supported bridge pier portfolio subjected to different seismic scenarios. The first model (ANN-1) captures the interrelationships among different IMs, the second model (ANN-2) predicts structural responses, and the third model (ANN-3) estimates structural capacity, specifically, the limit point on the pushover curve, based on geometric and material input parameters, thus enabling the explicit incorporation of epistemic uncertainty. These models are subsequently integrated into a Monte Carlo simulation scheme to generate fragility curves across multiple damage states. This approach significantly improves computational efficiency while maintaining high accuracy, offering a scalable and practical solution for seismic risk assessment and performance-based bridge design. Notably, the proposed framework is tailored and validated for bridge pier systems, capturing their unique structural behaviors, and introduces a novel capacity modeling strategy via ANN-3 that allows fragility curves to reflect both seismic demand variability and structural capacity randomness. Together, this enables a more robust and realistic evaluation of seismic vulnerability by addressing key limitations of conventional assessment approaches. Specifically, the integration of detailed nonlinear modeling with an ML-based framework allows for the efficient handling of complex structural behaviors and uncertainties across large bridge portfolios. This capability is especially valuable for applications requiring rapid, large-scale assessments, where traditional simulation-based methods may be computationally prohibitive. Moreover, by facilitating the prediction of both structural demand and capacity without assuming predefined probability distributions, the framework supports resilience-based decision-making that considers not only immediate damage but also long-term functionality and recovery. As a result, the proposed approach enhances the accuracy, scalability, and practical utility of seismic risk assessments for critical infrastructure systems.

2. Development of fragility curves using an ANN series-based model

2.1. Methodology

A series-distributed ANN workflow for constructing fragility curves of RC bridge piers is proposed. ANN-1 learns correlations among IMs from a limited feature set; ANN-2 predicts drift demand conditioned on IMs and modeling parameters; ANN-3 estimates damage-state drift thresholds from capacity information. Coupled with Monte Carlo sampling, the three surrogates yield fragility across multiple damage states without imposing lognormal forms on demand or capacity. The procedure is summarized in Fig. 1 and detailed below.

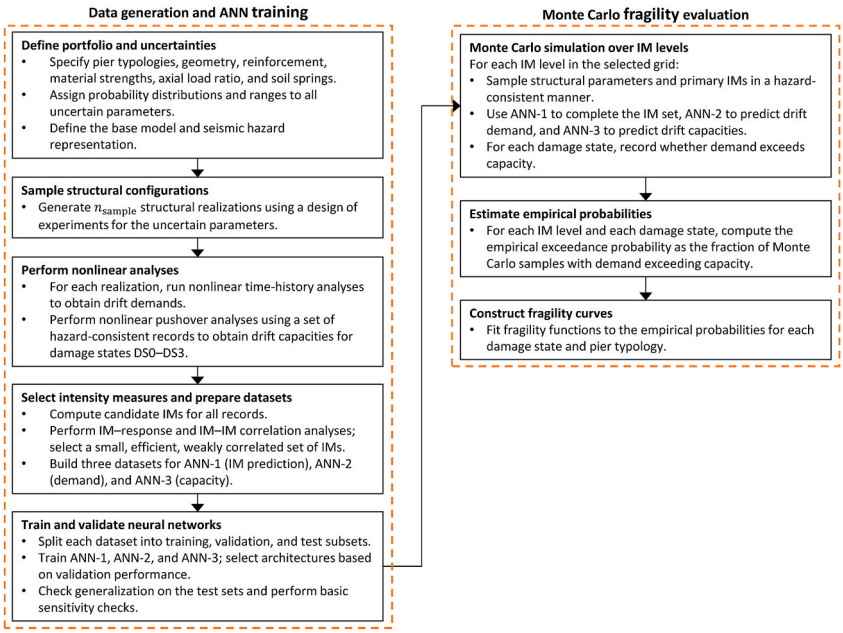

Fig. 1. Process for constructing the fragility curve using a series of ANN models.

- Step 1 - Define portfolio and uncertainties: An OpenSees finite element model of the RC bridge pier is first developed, incorporating material nonlinearity, bearings, and equivalent soil springs. Pier typologies (rectangular and circular), geometry, reinforcement, material strengths, axial load ratio, and foundation properties are specified, and probability distributions with associated ranges are assigned to all uncertain parameters. The seismic hazard representation, in terms of uniform hazard spectra and selected ground-motion sets, is also defined.
- Step 2 - Sample structural configurations: A design of experiments (DoE) approach is then employed to generate n_{sample} structural realisations for each pier typology by sampling the uncertain geometric and material parameters within the prescribed ranges.
- Step 3 - Perform nonlinear analyses: For every realization, nonlinear time-history analyses are carried out with the selected ground-motion records to obtain peak drift ratios and other response quantities, and nonlinear pushover analyses are performed to derive capacity curves and to identify drift capacities associated with damage states DS0–DS3 (slight, moderate, extensive, and complete).
- Step 4 - Select IMs and prepare datasets: Candidate IMs for all records are computed. IM–response and IM–IM correlation analyses are then used to select a small, efficient, and weakly correlated IM subset. On this basis, three datasets are assembled: one for ANN-1, in which primary IMs serve as inputs and the remaining IMs as outputs; one for ANN-2, in which IMs and structural parameters form the inputs and drift demand is the output; and one for ANN-3, in which structural parameters are the inputs and drift capacities for DS0–DS3 are the outputs.
- Step 5 - Train and validate neural networks: Each dataset is split into training, validation, and test subsets, and ANN-1, ANN-2, and ANN-3 are trained and tuned using the validation sets. Prediction accuracy is finally assessed on the test sets, and basic sensitivity checks are performed to confirm that the influence of the input variables is consistent with structural mechanics.
- Step 6 - Monte Carlo simulation over IM levels: A grid of IM levels is defined to cover the hazard range of interest. For each IM level, structural parameters are sampled from their probability distributions, and primary IMs are sampled in a hazard-consistent manner. The sampled variables are then passed through the trained networks: ANN-1 is used to complete the IM vector, ANN-2 to predict drift demand, and ANN-3 to predict drift capacities for all damage states.
- Step 7 - Estimate empirical probabilities: For each Monte Carlo sample and for each damage state, it is recorded whether the predicted drift demand exceeds the corresponding drift capacity. The empirical probability of exceedance at a given IM level is obtained as the fraction of samples for which exceedance occurs.
- Step 8 - Construct fragility curves: for each damage state and pier typology, a lognormal fragility function is fitted to the set of empirical probabilities over the IM grid.

2.2. Data generation and features

To construct the training datasets for the ANN-1 and ANN-2 models, numerical simulations based on nonlinear time-history

Table 1
Selected IMs used in this study.

No	IM	Note
Magnitude-based IMs		
1	$PGA = max\|a(t)\|$	Peak ground acceleration – Defined as the maximum absolute value of ground acceleration $a(t)$ over the time-history.
2	$PGV = max\|v(t)\|$	Peak ground velocity – Defined as the maximum absolute value of ground velocity $v(t)$ over the time-history.
3	$PGD = max\|d(t)\|$	Peak ground displacement – Defined as the maximum absolute value of ground displacement $d(t)$ over the time-history.
Frequency content-based IMs		
4	$Sa(T_1)$	Spectral acceleration at the fundamental period T_1 – The acceleration response spectrum at the structure's fundamental period.
5	$Sv(T_1)$	Spectral velocity at the fundamental period T_1 – The velocity response spectrum at the structure's fundamental period.
6	$Sd(T_1)$	Spectral displacement at the fundamental period T_1 – The displacement response spectrum at the structure's fundamental period.
7	$ASI = \int_{0.1}^{0.5} Sa(T)dT$	Spectral acceleration intensity – An integrated measure of the spectral acceleration over a range of periods.
8	$VSI = \int_{0.1}^{2.5} Sv(T)dT$	Spectral velocity intensity – An integrated measure of the spectral velocity over a range of periods.
9	$Sa^* = Sa(T_1)]^{1-\alpha} Sa(T_f)]^{\alpha}$	A spectral acceleration measure that accounts for spectral shape, considering softening effects where T_f is the period shift due to stiffness degradation, with $\alpha = 0.5$ and $T_f = 2T_1$.
10	$Sa_{AV} = \left[\prod_{i=1}^{n} Sa(T_i)\right]^{1/n}$	Average ground acceleration spectrum, where a series of cycles between $0.2T_1$ and $2T_1$ with a cycle step of 0.01s is used
11	$I_{NP} = Sa(T_1)\left(\frac{Sa_{AV}(T_1 \ldots T_n)}{Sa(T_1)}\right)^{\alpha}$	A modified spectral acceleration measure considering spectral shape effects, where the longest period considered is $T_n = 2T_1$ and $\alpha = 0.4$.
Duration-based IMs		
12	$I_A = \frac{\pi}{2g}\int_0^{t_f} [a(t)]^2 dt$	Arias intensity – A measure of the earthquake energy intensity, where tft represents the duration of ground motion (total length of the acceleration record).
13	$P_A = \frac{1}{t_D}\int_{t_5}^{t_{95}} a^2(t)dt$	Housner intensity – Defined as the integral of spectral velocity over a specific range, where $t_D = t_{95} - t_5$ is the strong motion duration (with t_5 and t_{95} being the time corresponding to 5 % and 95 % of the Arias intensity).
14	$I_C = a_{rms}^{1.5} t_D^{0.5}$	Characteristic Intensity – Defined as the root mean square of acceleration $a_{rms} = \sqrt{P_A}$.
15	$CAV = \int_0^{t_f} \|a(t)\|dt$	Cumulative absolute velocity – The integral of absolute acceleration over time, used to quantify the severity of ground motion.
16	$CAD = \int_0^{t_f} \|v(t)\|dt$	Cumulative absolute displacement – The integral of absolute displacement over time, capturing long-period motion effects.

analyses are performed on the generated finite element model realisations. These analyses employed a suite of hazard-consistent ground motion records selected based on site-specific seismic hazard characteristics for a representative range of IMs. The resulting structural response data, along with the corresponding IMs, serve as the foundation for training and validating both ANN-1 and ANN-2. Together, these models enable efficient prediction of structural responses, following the procedure outlined in Section 2.1.

The fragility curve of a structure can be constructed using various IMs, depending on the selected seismic hazard model. In this study, PGA and $Sa(T_1)$ are chosen as the primary IMs for fragility curve development. These IMs are widely adopted in performance-based seismic design due to their popularity and often a good correlation with structural response. However, it is important to note that the effectiveness of different IMs can vary significantly, depending on their ability to capture relevant aspects of ground motion characteristics [29].

To ensure a comprehensive evaluation, a total of 16 IMs were considered and categorized into three groups based on their physical significance, as shown in Table 1: (i) IMs related to ground motion amplitude, (ii) IMs associated with frequency content, and (iii) IMs characterizing the duration of shaking. The aim was to identify the most informative IMs from each category to establish robust predictive ANN models. These IMs were carefully selected to cover a broad spectrum of seismic characteristics, enhancing the reliability of the bridge pier's performance assessment [29].

Following the nonlinear time-history analyses, a dataset consisting of IMs and their corresponding structural response quantities was developed. A correlation analysis was then conducted to evaluate the relationship between each IM and the structural response metrics. This analysis enabled the selection of the most influential IMs, which serve as input features for ANN model development. A well-correlated input vector improves the prediction accuracy of ANN models while also reducing complexity. Features with a weak or very strong correlation with the output were excluded to avoid overfitting and enhance generalization capabilities.

Based on this process, two distinct datasets were developed for training ANN-1 and ANN-2.

- Dataset 1 (for ANN-1) includes *PGA*, $Sa(T_1)$ and the top-performing IMs from each group, selected based on their correlation with structural response through a Pearson correlation analysis.
- Dataset 2 (for ANN-2) extends Dataset 1 by incorporating structural modeling parameters (e.g., geometric and material properties), with the structural response as the output target.

Additionally, a separate dataset was prepared for training ANN-3, which is designed to predict the structural damage thresholds corresponding to predefined damage states. To generate this dataset, nonlinear static (pushover) analyses were performed by systematically varying the structural parameters listed in Tables 2 and 3. For each configuration, the associated damage thresholds were derived from the structural capacity curves.

These datasets collectively support the training of the three ANN models: ANN-1 and ANN-2 predict structural response as a function of seismic input parameters, while ANN-3 maps structural modeling parameters to corresponding damage state thresholds, enabling a data-driven approach for fragility evaluation.

2.3. Monte Carlo fragility construction

At this stage, the fragility curves of the RC bridge pier can be efficiently generated by integrating the trained ANN models within a Monte Carlo simulation framework. Fragility at intensity level x is defined as the conditional probability that structural demand D exceeds capacity C_k for damage state k,

$$P[\mathrm{DS} \geq k | \mathrm{IM} = x] \approx \frac{1}{N} \sum_{i=1}^{N} \mathbf{1}\left(D_i(x, \boldsymbol{\theta}_i) \geq C_{k,i}(\boldsymbol{\theta}_i)\right), \tag{1}$$

$$\mathbf{1}\left(R_i(x, \boldsymbol{\theta}_i) \geq C_{k,i}(\boldsymbol{\theta}_i)\right) = \begin{cases} 1, & \text{if the event "demand} \geq \text{capacity for DS } k\text{" is true for sample } i \\ 0, & \text{otherwise.} \end{cases}$$

where $\boldsymbol{\theta}_i$ are sampled geometric/material parameters representing epistemic variability. For each Monte Carlo realization, ANN-1/ANN-2 predict D_i conditioned on IMs and modeling parameters, and ANN-3 provides $C_{k,i}$ from the capacity dataset. No distributional form is prescribed for D or C_k; the probability emerges from sampling and surrogate predictions.

In the present framework, fragility information is obtained in a non-parametric manner. For each *PGA* level, the exceedance

Table 2
Range and distribution function of random input parameters for rectangular cross-section bridge columns.

No.	Input parameter	Minimum value	Maximum value	Distribution
1	Column cross-section depth, H (m)	0.5	3.0	Uniform
2	Ratio of column width to cross-section depth, B/H	1	3	Uniform
3	Ratio of column length to cross-section depth, L/H	2.0	8.0	Uniform
4	Axial force ratio, $P/f_c'A_g$	0.01	0.2	Uniform
5	Concrete compressive strength (MPa), f_c'	20	40	Uniform
6	Yield strength of longitudinal reinforcement (MPa), f_{yl} (MPa)	300	400	Uniform
7	Longitudinal reinforcement ratio, ρ_l	0.5 %	2 %	Uniform

Table 3
Range and distribution function of random input parameters for circular cross-section bridge columns.

No.	Input parameter	Minimum value	Maximum value	Distribution
1	Column diameter, D (m)	0.5	3.0	Uniform
2	Ratio of column length to cross-section depth, L/H	2.0	8.0	Uniform
3	Axial force ratio, $P/f_c'A_g$	0.01	0.2	Uniform
4	Concrete compressive strength (MPa), f_c'	20	40	Uniform
5	Yield strength of longitudinal reinforcement (MPa), f_{yl} (MPa)	300	400	Uniform
6	Longitudinal reinforcement ratio, ρ_l	0.5 %	2 %	Uniform

probability is first computed directly from the Monte Carlo samples as the empirical frequency of realisations with drift demand exceeding drift capacity. No distributional form is assumed for either demand or capacity in this step. A lognormal cumulative distribution is then fitted to these empirical points using a fitting procedure only as a smoothing and parametrization device, so that the underlying fragility estimation is not dependent on the lognormal assumption.

In addition, within this framework, two sources of uncertainty are involved. Aleatory uncertainty is associated with record-to-record variability of ground motions within each hazard level and is represented by the ensemble of selected and scaled records. Epistemic uncertainty is associated with incomplete knowledge of the portfolio properties and is represented by the DoE of geometric and material parameters (column dimensions, reinforcement ratios, material strengths, axial load index) within the ranges reported in Tables 2 and 3. The resulting fragility curves therefore reflect the combined effect of aleatory and epistemic variability, that is, total uncertainty in the seismic demand–capacity ratio.

3. A case study of simply supported bridges in the Da Nang area

3.1. Determination of random input parameters and model sampling

A portfolio of simply supported RC bridges in Da Nang with rectangular or circular pier sections (Fig. 2) is considered. To support portfolio-scale screening, geometric and material parameters are modeled as random variables within practice-based bounds. This assumption is adopted due to the limited availability of detailed probabilistic data, with the uniform distribution offering a practical means to represent parameter variability by assigning equal likelihood to all values within specified bounds [30].

The lower and upper bounds for these parameters are presented in Tables 2 and 3 for rectangular cross-section columns and for circular cross-section columns. Specifically, seven input parameters are defined for rectangular cross-sections, while six are specified for circular ones. To efficiently sample the input space and capture the influence of multiple uncertain variables, Latin hypercube sampling (LHS) method is employed for experimental design. This stratified sampling technique ensures a more uniform and representative distribution of samples across the entire range of input values compared to simple random sampling, thereby improving the accuracy and reliability of fragility analysis. Given the complexity of the model and the variability of the input parameters, a relatively large number of simulations is required to achieve statistically meaningful results. The number of model realisations was determined by considering (i) the dimensionality of the parameter space (number of geometric and material random variables), (ii) the need to achieve a balanced and representative coverage of that space via LHS, and (iii) the computational cost of nonlinear time-history and pushover analyses. A series of preliminary tests was performed in which the number of realisations was progressively increased (e.g., from 200, 300, 400, then to 500 per cross-section type), and the resulting ANN performance metrics and fragility estimates were compared. These tests showed that increasing the sample size from 300 to 500 realisations led to only marginal changes in the predicted fragility, indicating that the dataset had reached a stable level of representativeness. The selected number of realisations, therefore, reflects a compromise between adequate coverage of the input space and computational feasibility. Accordingly, a sample size of 300 realisations ($n_{\text{sample}} = 300$) is adopted, providing a balanced trade-off between computational efficiency and the robustness needed to capture the variability of structural response under seismic loading.

Fig. 2. An example of typical RC simply supported bridges with rectangular and circular cross-section columns in Da Nang.

3.2. Structural modelling of bridge piers

The RC pier columns are modeled and analyzed for seismic fragility evaluation using OpenSees [31]. A three-dimensional finite element model is developed, as illustrated in Fig. 3, in which a single-column pier is adopted as the basic structural unit for portfolio assessment and is subjected to the corresponding superstructure loading. For bridges with multi-column bents, each column is modeled individually with its tributary deck mass and boundary conditions, while mutual interaction between columns within a bent is not explicitly represented. The model incorporates key geometric and material parameters, along with appropriate boundary conditions to reflect realistic structural behavior. The column's fiber section is defined using uniaxial material models for both concrete and reinforcing steel, allowing for an accurate representation of nonlinear material behavior. At the top of the pier, the axial load from the superstructure is applied, calculated as $P = R_{sup}/n_{col}$, where R_{sup} is the total superstructure load per span and n_{col} is the number of columns.

Flexure-controlled assumption: To ensure reliable prediction of the seismic response, it is essential to identify the governing failure mode of the RC pier columns. Various methods for failure mode classification, ranging from empirical approaches to ML-based models, are available in the literature [28]. In this study, the ML-based approach proposed in Ref. [32] is employed to primarily determine the failure mechanisms of all pier configurations. The classification results indicate that the columns are predominantly flexure-controlled or flexure–shear, without brittle shear failures. In this context, the transverse reinforcement detailing (stirrup spacing, diameter, and yield strength) is relatively uniform and constrained within a narrow range by the design requirements, whereas parameters such as column height, axial load ratio, concrete strength, and longitudinal reinforcement ratio exhibit much larger variability and a more pronounced influence on drift capacity. To keep the dimensionality of the input space at a manageable level for the ANN models, variability in shear reinforcement was therefore not treated as an explicit random variable and was instead represented implicitly through a fixed, code-compliant detailing consistent with the reference designs.

SSI modeling: The interaction between the pier and its foundation is represented by an equivalent spring system located at the column base. This system comprises two springs for horizontal translation, one for vertical translation, and three for rotational degrees of freedom. Each spring is implemented using a "zeroLength" element with linear elastic uniaxial material models defined by stiffness values in the corresponding directions. In modelling soil–structure interaction, a single representative soil profile is adopted for the entire bridge portfolio, with equivalent spring stiffnesses at the column base derived from a reference OpenSeesPL analysis [33]. In particular, vertical and horizontal translational stiffnesses and the corresponding rotational stiffnesses are derived from a single-pile OpenSeesPL model, using the initial tangent of the axial curve for vertical stiffness and of the lateral curve for horizontal and rotational stiffnesses. It should be noted that this choice reflects the lack of detailed subsurface information for all sites and is intended to capture the primary effects of soil flexibility while keeping the model tractable for large-scale analysis. Using constant soil stiffness reduces the variability in natural periods that would otherwise arise from spatial variations in soil conditions; however, within the considered parameter space, the dominant contributors to period dispersion are column height and section properties, which still vary significantly. This simplification may therefore lead to a slight underestimation of the overall dispersion in fragility parameters and can be regarded as potentially non-conservative for sites with much softer or much stiffer soils than the reference profile. A fully probabilistic treatment of soil properties and associated soil–structure interaction, and its impact on epistemic uncertainty bands of the fragility curves, is left for future work.

Bearing modeling: Elastomeric bearings are represented as linear elastic springs connecting the pier cap to the deck, with

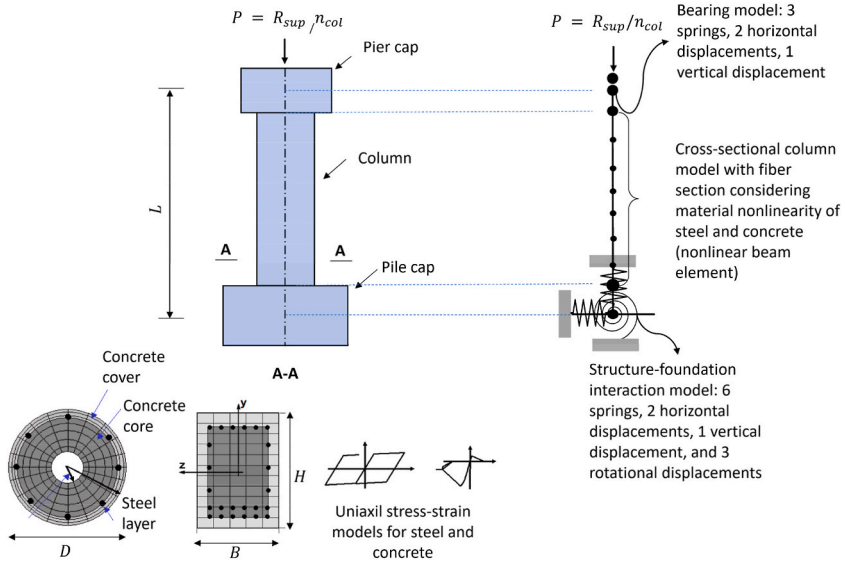

Fig. 3. Modeling bridge abutment structure considering the influence of bridge bearings and foundations (unit mm).

translational stiffness in the longitudinal and transverse directions and negligible rotational stiffness, consistent with the available design data. Approximate stiffness values are adopted in the analyses [7], and it is stated that these are intended to reflect typical code-compliant elastomeric bearings for the considered bridges.

Flexural fixity at column top and deck torsional stiffness: The column is connected to a pier cap modeled as a linear elastic beam element, and the combination of pier cap stiffness and bearing stiffness provides an effective rotational restraint at the column top. The torsional stiffness of the full deck is not modeled explicitly; instead, its influence is approximated through these boundary conditions. This modelling choice is consistent with a column-level analysis and is acknowledged as a simplifying assumption with respect to full three-dimensional deck behaviour.

The nonlinear time-history analyses are performed in the longitudinal direction of the bridge, which typically governs the seismic vulnerability of RC piers. A Rayleigh damping model is adopted for these analyses, and the Krylov–Newton algorithm is used as the solution strategy, with a fixed time step of 0.01 s employed for the integration of all ground-motion records.

3.3. Selection of ground motions for time-history analysis

A total of seven sets of ground motions were selected using the Scores algorithm proposed in Ref. [34]. Each set contains 20 three-component records, giving 140 records in total for the nonlinear time-history analyses used to generate training data for the ANN models. The study area is characterized by low–to–moderate seismic hazard [35]; to obtain motions with a sufficiently wide range of intensities capable of producing all considered damage states in the bridge columns, records were taken from the highly seismic region of Sicily (Italy). According to the seismic hazard curve (Fig. 4(a)), Uniform hazard spectra (UHS) were constructed for return periods $T_r = 75, 130, 240, 430, 780, 1400$, and 2500 years, as shown in Fig. 4(b). For each T_r, the Scores algorithm selected a set of records such that both the mean pseudo-acceleration response spectrum and the mean ± one standard deviation (approximately the 84th percentile) closely match the target UHS over the period band of interest. An example of the pseudo-acceleration spectra of the selected records, together with the target UHS for $T_r = 2500$ years is illustrated in Fig. 4(c).

3.4. Selection of engineering demand parameters and damage states

In this study, the drift ratio (δ) is adopted as the engineering demand parameter to evaluate the seismic performance of RC bridge

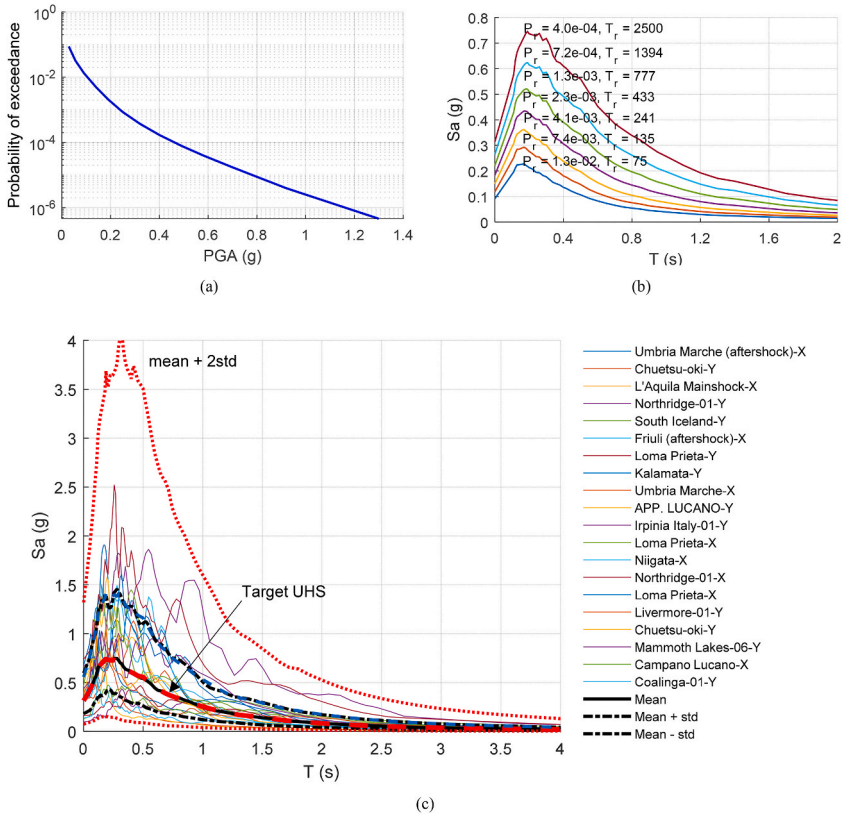

Fig. 4. (a) Seismic hazard curve, (b) UHS of different return periods, and (c) An example of pseudo-acceleration spectra of selected records corresponding to a UHS of $T_r = 2500$ years.

columns subjected to lateral earthquake loading. The damage states are classified based on specific drift thresholds corresponding to distinct physical and structural behaviors of the columns. These thresholds are typically derived from experimental results or standard design guidelines; however, in the absence of such data, they can be estimated through nonlinear static pushover analyses, as illustrated in Fig. 5. This figure presents a bilinear idealization of the shear force-drift ratio response, capturing the nonlinear characteristics of structural behavior and forming the basis for damage state classification.

Four key damage states are identified as characteristic points in Fig. 5.

- DS0 (Cracking damage): Assumed to occur at a drift ratio according to about 40 %–50 % of the peak shear force V_{peak} [36]. This state is associated with the initiation of flexural or diagonal cracking, typically with no significant strength degradation.
- DS1 (Slight damage): Defined at the yield point, where longitudinal reinforcement begins to yield. The corresponding drift ratio is determined using an idealized bilinear shear-drift curve constructed to equate the energy under the actual pushover response, as shown in Fig. 5 [37]. At this stage, minor plastic deformation occurs with limited residual displacement.
- DS2 (Moderate damage): Occurs near the peak lateral strength of the column; this state represents the maximum load-carrying capacity and is characterized by significant inelastic deformation and plastic hinge formation.
- DS3 (Extensive damage): Defined as the ultimate drift limit, where the shear strength degrades to 80 % of V_{peak}. At this point, the structure exhibits severe damage, including bar buckling, concrete spalling, and loss of lateral load resistance.

To predict the drift capacities associated with these damage states for pier columns with varying geometric and mechanical properties, a dedicated artificial neural network model (ANN-3) is developed. The model is trained using a dataset generated from nonlinear static pushover analyses performed on RC bridge columns subjected to longitudinal lateral loading. The predicted drift limits for DS0 to DS3 are then used for subsequent seismic fragility analysis.

3.5. Construction of the training datasets

To streamline modeling and analysis for a large number of samples, the Uqlab tool [38] within the MATLAB software platform is used in conjunction with the OpenSees software. Specifically, the Uqlab tool facilitates the definition and control of input parameters, value ranges, probability distributions, sampling techniques, and the number of samples directly within MATLAB. The static and nonlinear dynamic analysis processes on the OpenSees model are managed through the UQLab tool in the MATLAB environment, as illustrated in Fig. 6. In this workflow, nonlinear static pushover analyses are conducted to determine the damage states of the pier, corresponding to its performance levels. Additionally, nonlinear dynamic analyses are performed to assess the drift ratio of the column. For the dynamic analysis, the previously mentioned set of 140 selected accelerations is utilized. To perform the analysis across 300 models, the sequential numbers of the ground accelerations (n_{accel} = 1–140) are treated as random variables, following a uniform distribution. The results of a total of 300 dynamic analyses are then compiled to create datasets for training the ANN models.

For the portfolio analyzed, the first-mode period T_1 of the pier systems lies approximately in the range $T_{1,\min} \approx 0.157$ s to $T_{1,\max} \approx 2.664$ s for circular columns and $T_{1,\min} \approx 0.123$ s to $T_{1,\max} \approx 2.252$ s for rectangular columns, depending mainly on column height, cross-section dimensions, and foundation stiffness. The UHS and record-selection procedure described above are defined over a period interval that fully encompasses this T_1 range, ensuring consistency between the structural dynamic properties and the seismic input adopted in the time-history analyses.

Based on the static and nonlinear dynamic analysis results from the 300 models, a total of six datasets are created, three for each cross-section type. Specifically.

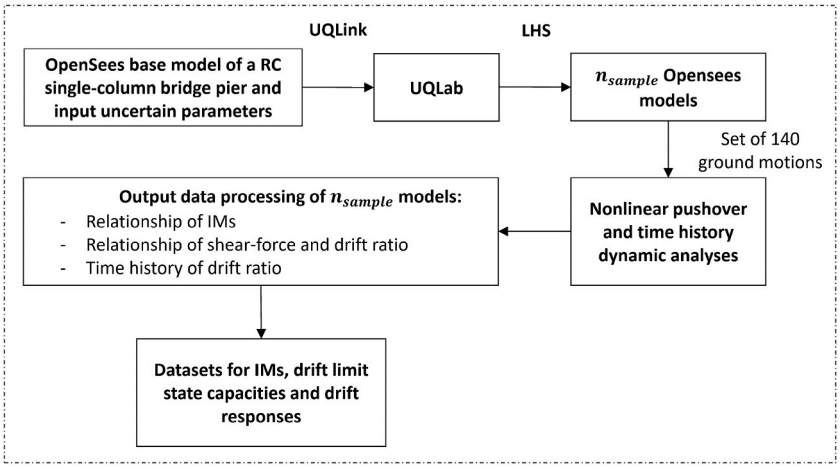

Fig. 5. Definition of damage states according to the nonlinear pushover analysis.

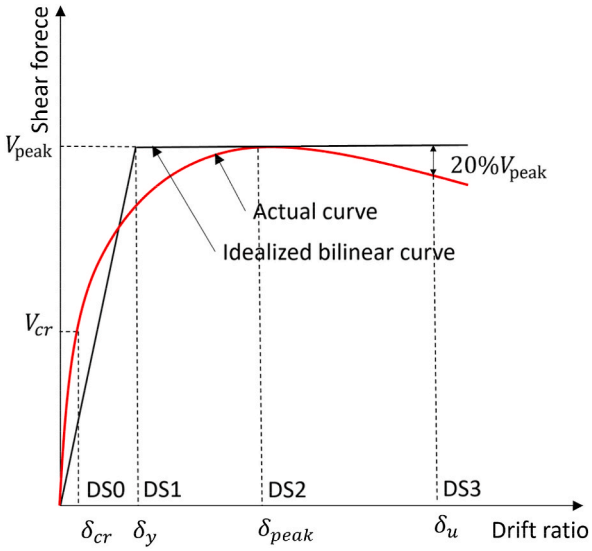

Fig. 6. Implementation of the OpenSees model in the Uqlab tool.

(i) IM dataset for training ANN-1:

Input: *PGA* and $Sa(T_1)$,
Output: Three IMs representing three IM groups from Table 1.

(ii) Dynamic response dataset for training ANN-2:

Input: Structural modeling parameters and IMs (*PGA*, $Sa(T_1)$, and three representative IMs from Table 1),
Output: Pier drift ratio (δ).

(iii) Static response dataset for training ANN-3:

Input: Structural modeling parameters.
Output: Four drift limits (δ_{cr}, δ_y, δ_{peak}, and δ_u).

The use of correlated IMs is acknowledged as a trade-off between parsimony and predictive performance; in principle, a more aggressive feature-selection or dimensionality-reduction strategy (e.g., clustering) could further reduce redundancy [22]. In this study, a correlation-based feature-selection procedure was applied to identify a compact IM set for ANN-2 from IMs in Table 1. Pearson correlation coefficients were first computed between each candidate IM and the drift demand, together with the full IM–IM correlation matrix. Within each physical group (amplitude-, frequency-, and duration-related IMs), IMs with $|\rho_{\text{IM,Demand}}| < 0.70$ were discarded. The remaining IMs were then ranked using the score

$$S_i = |\rho_{\text{IM,Demand}}| - \lambda_j \in S_{\max} |\rho_{ij}|, \tag{2}$$

where S initially contains the primary IMs PGA and $Sa(T_1)$, $\rho_{\text{IM,Demand}}$ is the IM–demand correlation, ρ_{ij} are IM–IM correlations, and $\lambda = 1.0$ penalises redundancy. For each group, the IM with the highest score was chosen. This procedure selected *PGV* as the representative amplitude-based IM, *VSI* as the representative frequency-based IM, and I_c as the representative duration-based IM, which are used together with PGA and $Sa(T_1)$ as inputs to ANN-2. The selected IMs exhibit strong correlation with drift demand while maintaining only moderate mutual correlation, thereby balancing predictive efficiency and parsimony. This choice is subsequently examined and supported by an ANN-based sensitivity analysis assessing the effectiveness of both structural and IM parameters in governing the structural demand.

3.6. Training, validation, and sensitivity analysis of the ANN models

To assess the predictive capability of the neural networks and avoid overfitting, the available dataset is partitioned into three disjoint subsets: a training set (80 %), a validation set (10 %), and an out-of-sample test set (10 %). The training set is used to calibrate the network weights, while the validation set guides the selection of the number of hidden neurons and other hyperparameters. The final performance of each ANN is then evaluated on the test set, which is not involved in any stage of model development. The chosen 80-10-10 split is particularly suitable for medium-to-large datasets, minimizing the risk of overfitting while preserving

generalizability.

In this study, a system comprising three trainable cascade-forward backpropagation networks arranged in series is employed. The cascade-forward structure extends the feedforward architecture by incorporating direct connections from the input layer to all subsequent layers, improving convergence speed and the ability to capture complex input–output mappings. Each network contains two hidden layers, selected to provide adequate model complexity while avoiding unnecessary overparameterization. The activation functions are chosen based on their known benefits in nonlinear modeling: the positive linear (poslin) function is applied in ANN-1 and ANN-3 to ensure non-negative, linear output responses suited for regression tasks, while the log-sigmoid (logsig) function in ANN-2 introduces nonlinearity and bounded outputs, aiding the network in capturing subtle relationships within normalized data.

Training is conducted using the Levenberg-Marquardt algorithm (trainlm), a second-order optimization method known for its efficiency in training medium-sized networks with high precision. The mean squared error (MSE) is used as the loss function due to its interpretability and common usage in regression problems, reflecting the average squared difference between predicted and actual values. The overall network configuration (shown in Fig. 7) is designed to optimize predictive accuracy and learning stability across diverse model variants (ANN-1 to ANN-3) while maintaining consistency in the training and evaluation pipeline.

The training and validation processes are conducted using MATLAB software with the following basic parameters.

- Maximum number of epochs: 1000
- Minimum performance: 0
- Learning rate: 0.01
- Learning rate increase ratio: 1.05
- Learning rate reduction ratio: 0.7
- Minimum performance slope: 1×10^{-5}

As a result, four distinct ANN models were developed to estimate the nonlinear static and dynamic responses of the bridge columns. For each model, the network architecture was systematically evaluated by varying the number of neurons per hidden layer, ranging from 1 to 30 neurons, as detailed in Table 4. The optimal network architecture was determined by evaluating the achieved performance goal (MSE) of each model during the validation process, and finally was evaluated with the test dataset according to R^2 and *RMSE* metrics; therefore, reflect both in-sample and out-of-sample accuracy, demonstrating that the trained networks generalize satisfactorily beyond the training data.

In addition, a sensitivity analysis based on the connection-weights (Garson) method is performed for ANN-2 and ANN-3, and the resulting relative importance of input variables [39], as reported in Table 5, provides further insight into model behaviour. For ANN-2,

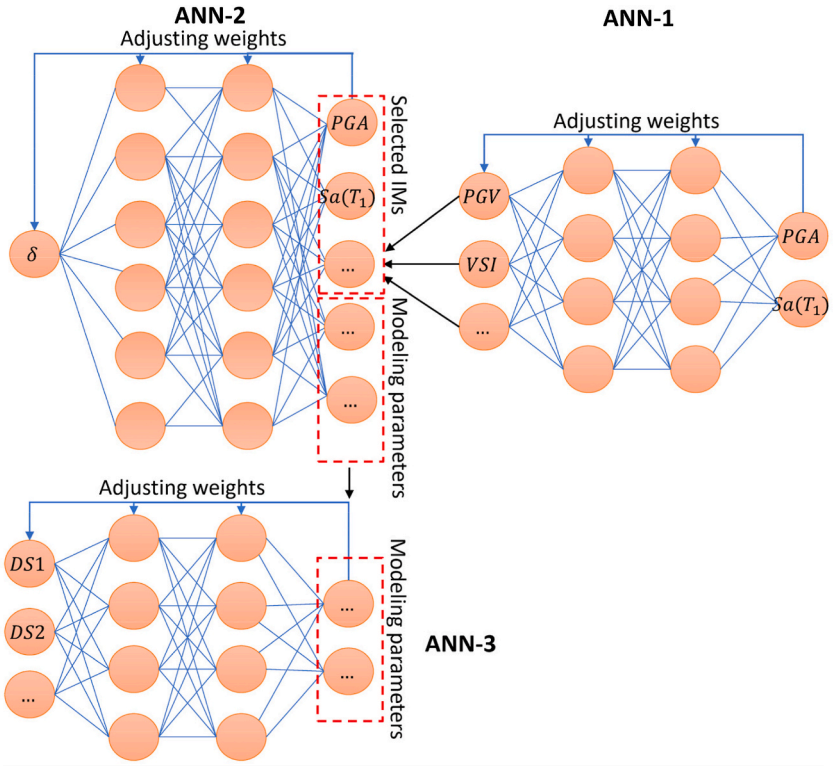

Fig. 7. A series of 3 trainable cascade-forward backpropagation neural networks with 2 hidden layers.

Table 4
The evaluation results of the ANN models.

Section	ANN model	Number of hidden layers	Neurons per hidden layer	Testing	
				R^2	RMSE
Rectangular	ANN model for IMs (ANN-1)	2	7	0.951	1.991
	ANN model for structural response (ANN-2)	2	29	0.943	0.075
	ANN model for damage states (ANN-3)	2	7	0.926	0.015
Circular	ANN model for IMs (ANN-1)	2	7	0.951	1.991
	ANN model for structural response (ANN-2)	2	12	0.935	0.088
	ANN model for damage states (ANN-3)	2	19	0.925	0.016

Table 5
Sensitivity of each input of trained ANN-2 and ANN-3 using the connection-weights (Garson) method.

Input variable											
H	B/H	L/H	$P/f_c'A_g$	f_c'	f_{yl}	ρ_l	PGA	$Sa(T_1)$	PGV	VSI	I_C
Relative importance (%) – ANN 2											
10.57	6.58	8.38	9.08	7.59	7.79	6.64	7.81	8.87	9.30	9.47	7.92
Relative importance (%) – ANN 3											
19.48	13.35	11.18	12.80	13.19	15.92	14.09					

the importance values are relatively balanced among geometric ratios (H, B/H, L/H), axial load ratio $P/f_c'A_g$, material strengths (f_c', f_{yl}), longitudinal reinforcement ratio ρ_l, and the selected IMs (PGA, $Sa(T_1)$, PGV, VSI, I_c), indicating that drift demand is governed by a combination of structural characteristics and ground-motion intensity, as expected from structural mechanics. For ANN-3, the highest relative importance is assigned to column height H and axial load ratio $P/f_c'A_g$, followed by concrete strength and reinforcement parameters, which are consistent with the dominant role of slenderness, axial load, and sectional capacity in controlling drift limits and damage-state thresholds. The ranking and magnitude of these importance measures confirm that the networks respond to parameter variations in a physically meaningful way, thereby supporting their suitability for portfolio-scale fragility prediction.

3.7. Structural response estimation and fragility curves

After training and validation, Monte Carlo simulations to generate fragility curves for four damage states (DS0–DS3) are performed. For each IM level within the hazard-consistent range, ANN-1/ANN-2 predict drift demand and ANN-3 supplies capacity thresholds; exceedance probabilities are then estimated empirically. The overall procedure is summarized in the following pseudocode.

```
Input:
    Trained networks: ANN-1 (additional IMs), ANN-2 (drift demand), ANN-3 (drift capacities)
    Number of Monte Carlo samples per IM level: n_samples = 10000
    PGA levels: PGA_j = 0.005 g: 0.005 g: 0.10 g//hazard-consistent range
    Lognormal model for Sa(T1) | PGA:
      Sa(T1) ~ Lognormal(μ = ln(PGA_j), σ = 1.0)
  Output:
    Empirical exceedance probabilities P(DSk | PGA_j) for damage states DS0–DS3
    Fitted fragility curves for each damage state
  Algorithm:
  for each PGA_j in [0.005 g, 0.010 g, …, 0.10 g] do
  //initialise exceedance counters for four damage states
    for k = 0 to 3 do
      N_exceed[k] = 0
    end for
  //Monte Carlo loop at this IM level
    for i = 1 to n_samples do
  //sample spectral acceleration at the first-mode period
      Sa_T1_i = sample_lognormal(μ = ln(PGA_j), σ = 1.0)
  //predict additional IMs (e.g., PGV, VSI, Ic)
      IM_add_i = ANN-1(PGA_j, Sa_T1_i)
  //assemble input vector for demand prediction
    x_demand_i = [PGA_j, Sa_T1_i, IM_add_i]
  //predict drift demand
    D_i = ANN-2(x_demand_i)
  //assemble input vector for capacity prediction
    x_cap_i = structural_parameters_for_sample_i//fixed or sampled as needed
```

(*continued on next page*)

(*continued*)

```
//predict drift limits for DS0–DS3
  C_i[00.3] = ANN-3(x_cap_i)
//check exceedance for each damage state
  for k = 0 to 3 do
  if D_i > C_i[k] then
    N_exceed[k] = N_exceed[k] + 1
    end if
  end for
  end for
//empirical exceedance probabilities at PGA_j
  for k = 0 to 3 do
    P(DSk | PGA_j) = N_exceed[k]/n_samples
  end for
end for
//for each damage state k, fit a lognormal fragility curve
//to [(PGA_j, P(DSk | PGA_j))] over all PGA_j
```

As an illustration, 100 Monte Carlo simulations are carried out for each *PGA* increment of 0.05 g. The statistical outcomes corresponding to the four damage states (DS0–DS3) obtained from these simulations are summarized in Fig. 8, where the blue circle markers represent the rectangular columns and the red dot markers represent the circular ones. To further illustrate the efficiency and behaviour of the proposed framework, Fig. 9 compares, for both rectangular and circular columns, the fragility curves obtained from the empirical Monte Carlo probabilities, their lognormal fit by means of the maximum-likelihood Probit-regression method proposed by Baker [40], and the traditional cloud-analysis procedure [7] for both rectangular and circular columns. For all damage states, the Monte Carlo points form smooth, monotonic trends of exceedance probability with PGA, and the corresponding solid curves obtained by lognormal fitting track these points closely over the entire intensity range. This consistency shows that the ANN–Monte Carlo framework provides internally coherent, essentially non-parametric fragility estimates and that the subsequent lognormal fit acts mainly as a mild smoothing step, without appreciably altering the underlying probabilities.

By contrast, the dashed curves from cloud analysis display a different behaviour. For DS0, the cloud-based fragilities rise more steeply at low PGA and reach high probabilities earlier than the Monte Carlo-based curves, indicating a tendency to overestimate the onset of minor damage. For DS1, the cloud curves generally lie below the Monte Carlo-based curves over a broad PGA range, underestimating the likelihood of slight-to-moderate damage at intermediate intensities. For DS2 and DS3, the differences are smaller but remain visible, with the cloud curves typically predicting higher probabilities at larger PGA and thus a steeper approach to unity. Taken together, Fig. 9(a) and (b) show that relaxing the internal lognormal assumption allows the fragility functions to follow the shape implied by the simulated demand–capacity ratios, whereas the cloud-based approach enforces a more rigid lognormal form that can either under- or over-estimate exceedance probabilities depending on the damage state, intensity level, and column typology.

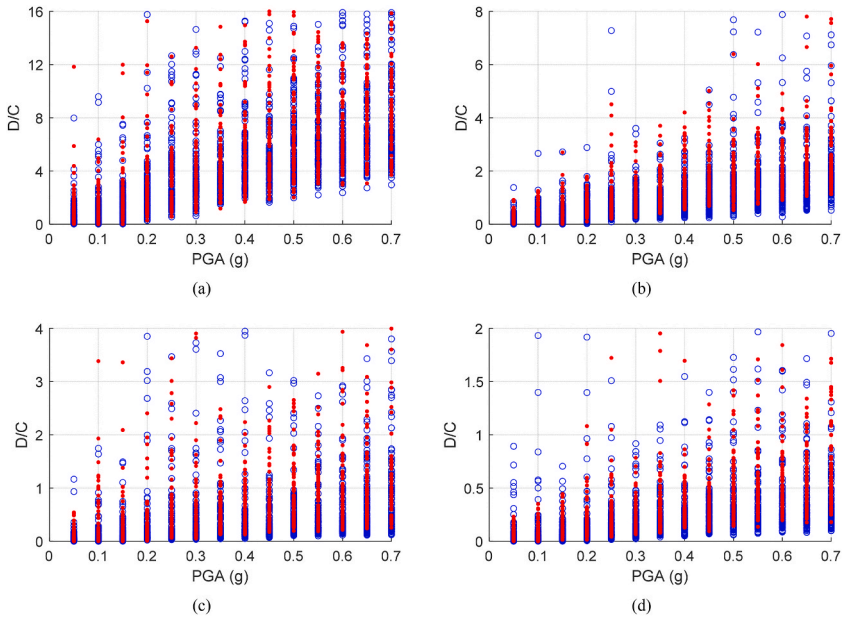

Fig. 8. An example of ANN series-based Monte Carlo simulations for four damage states of rectangular (blue circle) and circular (red dot) columns: (a) DS0, (b) DS1, (c) DS2, (d) DS3.

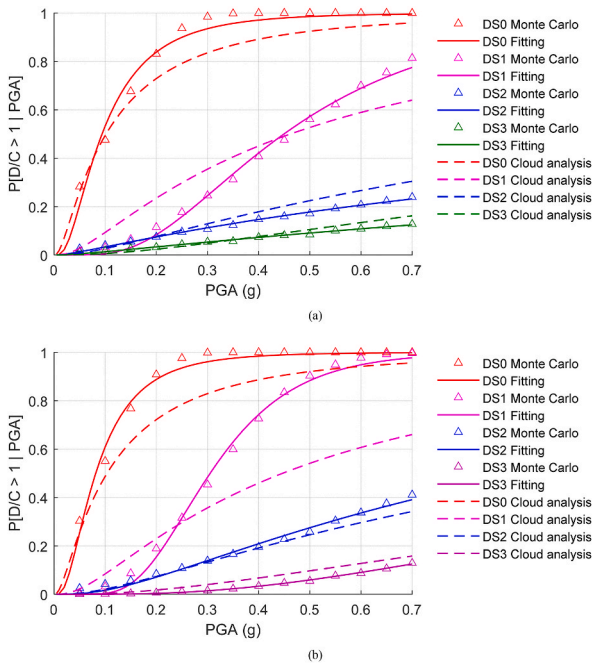

Fig. 9. A comparison of seismic fragility curves for different damage states of a system of simply supported RC bridges in the Da Nang area: (a) rectangular columns and (b) circular columns.

Building on the above results, Fig. 10 compares the ANN–Monte Carlo fragilities of rectangular and circular cross-sections. For all damage states, the curves for circular columns are in most cases steeper and shifted towards lower PGA values, indicating a tendency towards higher damage likelihood at a given intensity, particularly in the low-to-moderate PGA range. For DS0, the exceedance probability for circular columns increases very rapidly with PGA and reaches values close to unity at substantially lower PGA than for rectangular columns, reflecting an earlier onset of minor cracking and serviceability exceedance. For DS1, the circular-section fragility also rises more quickly, suggesting that moderate damage is more probable under relatively low shaking. The contrast becomes more pronounced for DS2, where the probability of extensive damage for circular columns grows markedly in the 0.2–0.5 g range, while rectangular columns display a more gradual increase. For DS3, exceedance probabilities remain relatively low over the considered PGA range for both typologies, although circular columns generally show slightly higher values. Some intersections between the rectangular and circular fragility curves are observed at specific PGA levels; these crossings reflect differences in both median capacity and dispersion, as well as variability within each portfolio, and indicate that strict stochastic dominance of one typology over the other is not implied across the entire intensity range. Nevertheless, the overall trend indicates that, on average, the circular piers in the considered portfolio exhibit higher fragility than the rectangular piers, with the magnitude of this vulnerability gap depending on the damage level and PGA range under consideration.

To demonstrate the flexibility and applicability of the proposed approach, a seismic fragility analysis is carried out for 4 bridges located along National Highway 1A in Da Nang. The selected bridges include the Lieu Chieu Bridge, New Nam O Bridge, Do Bridge, and Qua Giang Bridge, detailed in Table 6, each representing typical structural configurations found in the region.

The statistical parameters and probability distribution functions for the geometric and material properties of the pier columns in

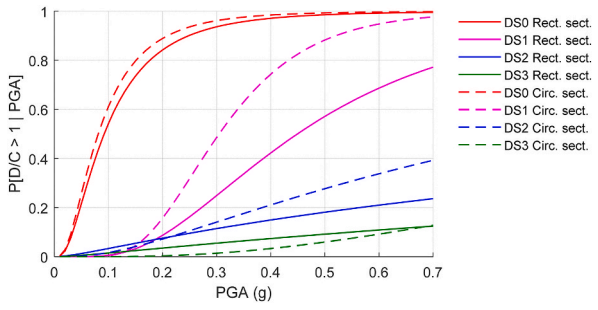

Fig. 10. Seismic fragility curves for different damage states of rectangular and circular RC pier columns of a system of simply supported RC bridges in the Da Nang area.

Table 6
Details of examined bridges along National Highway 1A in Da Nang.

No.	Bridge name	Bridge chainage (location)	Bridge type	Number of spans, span length	Main girder type	Bearing type	Column types
1	Lien Chieu Bridge	Km914 + 450 – National Highway 1	Simply supported PSC bridge	(3 × 12.5) m	PSC beam, fish-belly shape	Elastomeric bearing	Seven-column pier
2	New Nam Bridge	Km917 + 198 – National Highway 1	Simply supported PSC bridge	(8 × 40) m	Super-T PSC girder	Elastomeric bearing	Two-column pier
3	Do Bridge (approach spans only)	Km934 + 594 – National Highway 1	PSC bridge	(1 × 33) m	I-shaped PSC girder	Elastomeric bearing	Two-column pier
4	Qua Giang Bridge	Km938 + 980 – National Highway 1	Simply supported PSC bridge	(3 33) m	I-shaped PSC girder	Elastomeric bearing	Two-column pier

these bridge systems are defined based on available design documents and test data. Specifically, the concrete compressive strength (f'_c) and the thickness of the protective concrete cover (t_{cover}) are obtained from experimental testing, ensuring an accurate representation of actual field conditions. For each random input variable, the appropriate probability distribution function is assigned, and with the associated parameters. As summarized in Table 7, most variables are modeled using uniform distributions with lower and upper values, reflecting the lack of detailed probabilistic data. However, key material properties such as concrete compressive strength and steel yield strength are modeled using normal distributions with mean and standard deviation, in accordance with common engineering practice and based on available statistical test results.

Following the aforementioned steps, Monte Carlo simulations are performed for each specified PGA level, allowing the rapid generation of fragility curves corresponding to four damage states for the pier columns in the bridge system, as shown in Fig. 11. This process highlights the robustness and flexibility of the proposed approach, as it enables the efficient derivation of fragility curves without the need for repeated finite element simulations, detailed structural analyses, or pre-defined probability distributions for structural demand, capacity, or IMs.

Since the fragility analysis is performed at the single-column pier level, the resulting pier fragilities can be used as building blocks for bridge-level fragility curves. For bridges where failure of a single pier is critical (e.g., single-pier bents or configurations in which loss of any pier leads to loss of serviceability), the bridge fragility can be approximated by the fragility of the most critical pier or by the envelope of pier-level fragilities. For multi-span, multi-pier bridges, different system idealisations are possible. A conservative option is to model the bridge as a series system, where the probability of exceeding a damage state is obtained by combining pier-level fragilities under the assumption that failure of any pier governs; more refined approaches may allow for partial damage tolerance and would require explicit system reliability modelling. Such system-level formulations are beyond the scope of the present study, but the ANN-based column fragilities developed here are intended to serve as fundamental input components for future bridge-level and network-level seismic risk assessments.

4. Conclusions

This study introduced a series-distributed ANN framework for portfolio-scale fragility analysis of RC bridge columns that explicitly represents epistemic uncertainty in both seismic demand and capacity, relaxes restrictive distributional assumptions, and substantially reduces computational cost. The framework comprises three interconnected cascade-forward backpropagation networks, each trained on datasets derived from nonlinear time-history and static pushover analyses. ANN-1 predicts secondary IMs from primary seismic inputs, ANN-2 estimates structural drift demands from IMs and geometric/material parameters, and ANN-3 forecasts drift-capacity thresholds for multiple damage states. Combined with Monte Carlo simulation, this three-model system enables efficient and accurate generation of fragility curves without embedding an internal lognormal assumption, thereby enhancing physical realism and interpretability.

Key contributions and findings can be summarized as follows.

- A comprehensive correlation analysis involving 16 IMs revealed that *PGV*, *VSI*, and I_C are the most effective predictors of drift demand for both rectangular and circular RC pier columns when used in combination with standard measures such as PGA and $Sa(T_1)$.
- The framework significantly reduces the computational burden of fragility assessment by substituting thousands of finite element simulations with well-trained ANNs. The surrogate models achieve excellent predictive accuracy, with R^2 values above 0.9 across all testing cases, validating their reliability for both static and dynamic response predictions. In particular, ANN-3 introduces a capacity-modelling approach based solely on geometric and mechanical characteristics, allowing the fragility curves to reflect variability in both seismic demand and drift capacity.
- In contrast to traditional approaches that assume lognormal distributions for both demand and capacity and derive fragility curves entirely within that parametric framework, this proposed framework derives fragility functions directly from data-driven simulation and prediction. Lognormal fragility functions are then fitted only as a post-processing step for smoothing and parameter extraction.
- The framework was successfully applied to a representative portfolio of simply supported RC bridges in Da Nang and four bridges along National Highway 1A in Vietnam. A connection-weights (Garson) sensitivity analysis for ANN-2 and ANN-3 shows that drift

Table 7
Determine the distribution type and corresponding parameters of the random variables.

Pier parameter	H (D) (m)	B/H	L/H	$P/(f'_c A_g)$	ρ_l	t_{cover} (mm)	f'_c (MPa)	f_y (MPa)
Distribution function	Uniform (lower and upper values)						Normal (mean and standard deviation)	
Distribution function parameters	0.709	1.000	3.296	0.019	0.008	35	30.512	360
	2.216	1.410	6.813	0.072	0.020	81	1.795	60

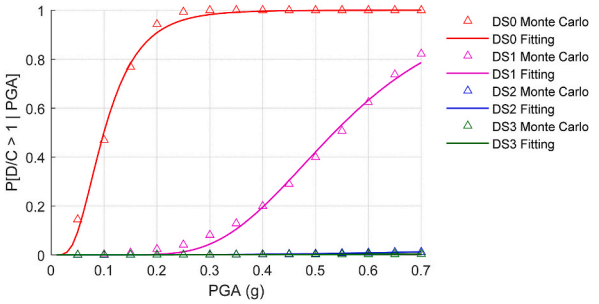

Fig. 11. Seismic fragility curves for different damage states of RC pier columns of 4 simply supported RC bridges in National Highway 1A through Da Nang.

demand is governed by a balanced combination of structural properties and IMs, whereas drift capacities are dominated by column height and axial load ratio, confirming that the networks respond to parameter variations in a mechanically consistent manner and are suitable for portfolio-scale fragility prediction.

- The resulting fragility curves for rectangular and circular piers show systematic differences in seismic vulnerability. Circular columns exhibit higher exceedance probabilities across damage states, especially at moderate-to-high PGA/IM levels, while rectangular sections are consistently less fragile over the same range. Compared with traditional lognormal-based fragility curves derived directly from cloud-analysis data, the non-parametric, ANN-driven fragility estimates yield broadly similar median capacities but noticeable differences in tail behaviour and dispersion for several damage states and pier geometries; thereby, highlighting the potential bias introduced by rigid lognormal assumptions in conventional fragility derivation.

In summary, the study establishes a powerful and generalisable framework for seismic fragility analysis of RC bridge columns that addresses key limitations of conventional methods. The combination of detailed nonlinear modelling, explicit epistemic uncertainty representation, and ML-based surrogate modelling results in a tool that is both computationally efficient and technically rigorous. It enables rapid, accurate, and scalable assessments of seismic vulnerability, which are crucial for large-scale infrastructure risk evaluations and policy-making in earthquake-prone regions. The approach is inherently scalable and adaptable, and can be extended to other bridge typologies, retrofitting scenarios, or larger infrastructure networks, as well as integrated into resilience-based decision frameworks requiring fast probabilistic estimates of demand and capacity under diverse seismic scenarios.

Future research should incorporate a more comprehensive treatment of soil–structure interaction and soil property variability, and investigate a clearer decomposition of epistemic and aleatory uncertainties, including the derivation of confidence intervals or bands for fragility parameters. In addition, extending the framework from single-pier idealisations to full bridge models will allow system-level seismic fragility and risk assessments, and will facilitate integration with network-level performance and accessibility metrics in multi-hazard contexts.

CRediT authorship contribution statement

Hoang Vinh Nguyen: Writing – original draft, Validation, Methodology, Investigation, Formal analysis, Data curation. **Hoang Nam Phan:** Writing – review & editing, Validation, Supervision, Methodology, Investigation, Formal analysis, Data curation, Conceptualization. **Duy Hoa Pham:** Writing – review & editing, Validation, Supervision. **Gianluca Quinci:** Writing – review & editing, Validation. **Fabrizio Paolacci:** Writing – review & editing, Validation.

Declaration of competing interest

The authors declare that they have no known competing financial interests or personal relationships that could have appeared to influence the work reported in this paper.

Acknowledgments

This study was supported by FABRE – Research consortium for the evaluation and monitoring of bridges, viaducts and other

structures (www.consorziofabre.it/en). Any opinion expressed in the paper does not necessarily reflect the view of the funder.

Data availability

The data and code generated or used during this study are available in a repository (https://data.mendeley.com/datasets/mf4s3tz68b/1).

References

[1] K.A. Porter, An overview of PEER's performance-based earthquake engineering methodology, in: Proceedings of Ninth International Conference on Applications of Statistics and Probability in Civil Engineering, 2003, pp. 1–8. Citeseer.
[2] J. Moehle, G.G. Deierlein, A framework methodology for performance-based earthquake engineering, in: 13th world conference on earthquake engineering 679, WCEE Vancouver, 2004, p. 12.
[3] C.A. Cornell, F. Jalayer, R.O. Hamburger, D.A. Foutch, Probabilistic basis for 2000 SAC federal emergency management agency steel moment frame guidelines, J. Struct. Eng. 128 (4) (2002) 526–533.
[4] D. Vamvatsikos, C.A. Cornell, Incremental dynamic analysis, Earthq. Eng. Struct. Dynam. 31 (3) (2002) 491–514.
[5] F. Jalayer, C. Cornell, Alternative non-linear demand estimation methods for probability-based seismic assessments, Earthq. Eng. Struct. Dynam. 38 (8) (2009) 951–972.
[6] Y. Pang, X. Wang, Cloud-IDA-MSA conversion of fragility curves for efficient and high-fidelity resilience assessment, J. Struct. Eng. 147 (5) (2021) 04021049.
[7] E. Choi, R. DesRoches, B. Nielson, Seismic fragility of typical bridges in moderate seismic zones, Eng. Struct. 26 (2) (2004) 187–199.
[8] P. Chomchuen, V. Boonyapinyo, Incremental dynamic analysis with multi-modes for seismic performance evaluation of RC bridges, Eng. Struct. 132 (2017) 29–43.
[9] S. Mangalathu, J.S. Jeon, Stripe-based fragility analysis of multispan concrete bridge classes using machine learning techniques, Earthq. Eng. Struct. Dynam. 48 (11) (2019) 1238–1255.
[10] H. Li, L. Li, G. Zhou, L. Xu, Effects of various modeling uncertainty parameters on the seismic response and seismic fragility estimates of the aging highway bridges, Bull. Earthq. Eng. 18 (14) (2020) 6337–6373.
[11] H. Li, A. Agrawal, Q. Chen, H. Wang, Numerical simulation of a long-span steel Truss Bridge subjected to blast loads, Int. J. Bridge Eng. Manag. Res. 2 (1) (2025), 21425009-1: 15.
[12] Y. Liu, D.-G. Lu, F. Paolacci, G. Quinci, S. Vern, Seismic resilience assessment for steel-concrete composite bridges including impacts of near-fault earthquakes, Int. J. Bridge Eng. Manag. Res. 1 (1) (2024), 21424005-1: 15.
[13] D.G. Giovanis, M. Fragiadakis, V. Papadopoulos, Epistemic uncertainty assessment using incremental dynamic analysis and neural networks, Bull. Earthq. Eng. 14 (2016) 529–547.
[14] Z. Wang, N. Pedroni, I. Zentner, E. Zio, Seismic fragility analysis with artificial neural networks: application to nuclear power plant equipment, Eng. Struct. 162 (2018) 213–225.
[15] Z. Liu, A. Sextos, A. Guo, W. Zhao, ANN-based rapid seismic fragility analysis for multi-span concrete bridges, Structures 41 (2022) 804–817.
[16] M.S. Razzaghi, M. Safarkhanlou, A. Mosleh, P. Hosseini, Fragility assessment of RC bridges using numerical analysis and artificial neural networks, Earthquake. Struct. 15 (4) (2018) 431–441.
[17] G. Quinci, N.H. Phan, F. Paolacci, On the use of artificial neural network technique for seismic fragility analysis of a three-dimensional industrial frame, in: Pressure Vessels and Piping Conference, vol 86199, 2022. V005T08A013.
[18] J.-Y. Ding, D.-C. Feng, C. Galasso, Seismic fragility assessment of regional building portfolios using machine learning and Poisson binomial distribution, Int. J. Disaster Risk Reduct. 116 (2025) 105044.
[19] P.H. Nam, H.M. Hung, N.M. Hai, H.P. Hoa, Plastic Hinge modeling for seismic damage assessment of rectangular reinforced concrete columns based on artificial neural network, JSTCE 15 (7V) (2021) 119–130. Hanoi University of Civil Engineering (HUCE).
[20] Y. Pang, X. Dang, W. Yuan, An artificial neural network based method for seismic fragility analysis of highway bridges, Adv. Struct. Eng. 17 (3) (2014) 413–428.
[21] Z. Liu, A. Guo, C. Zhao, A. Sextos, Seismic response of bridges employing knowledge-enhanced neural networks for the lumped plasticity modelling of RC piers, Bull. Earthq. Eng. 22 (7) (2024) 3393–3413.
[22] F. Parisi, A. Nettis, G. Uva, Machine learning-aided cloud analysis for seismic fragility assessment of multi-span bridges, Eng. Struct. 343 (2025) 121175.
[23] C. Karakostas, et al., Seismic assessment of bridges through structural health monitoring: a state-of-the-art review, Bull. Earthq. Eng. 22 (3) (2024) 1309–1357.
[24] G.C. Marano, M.M. Rosso, A. Aloisio, G. Cirrincione, Generative adversarial networks review in earthquake-related engineering fields, Bull. Earthq. Eng. 22 (7) (2024) 3511–3562.
[25] R. Monteiro, R. Delgado, R. Pinho, Probabilistic seismic assessment of RC bridges: part I—Uncertainty models, Structures 5 (2016) 258–273. Elsevier.
[26] S. Mangalathu, J.S. Jeon, R. DesRoches, Critical uncertainty parameters influencing seismic performance of bridges using Lasso regression, Earthq. Eng. Struct. Dynam. 47 (3) (2018) 784–801.
[27] A. Nettis, D. Raffaele, G. Uva, Seismic risk-informed prioritisation of multi-span RC girder bridges considering knowledge-based uncertainty, Bull. Earthq. Eng. 22 (2) (2024) 693–729.
[28] D. Herrera, G. Varela, D. Tolentino, Reliability assessment of RC bridges subjected to seismic loadings, Appl. Sci. 12 (1) (2022) 206.
[29] H.N. Phan, F. Paolacci, V.M. Nguyen, P.H. Hoang, Ground motion intensity measures for seismic vulnerability assessment of steel storage tanks with unanchored support conditions, J. Pressure Vessel Technol. 143 (6) (2021) 061904.
[30] G.P. Balomenos, S. Kameshwar, J.E. Padgett, Parameterized fragility models for multi-bridge classes subjected to hurricane loads, Eng. Struct. 208 (2020) 110213.
[31] F. McKenna, OpenSees: a framework for earthquake engineering simulation, Comput. Sci. Eng. 13 (4) (2011) 58–66.
[32] V.M. Nguyen, H.N. Phan, F. Paolacci, Feature selections and optimizable classification learners for detecting failure modes of rectangular reinforced concrete columns, Asia. J. Civil Eng. 24 (5) (2023) 1267–1281.
[33] J. Lu, A. Elgamal, Z. Yang, OpenSeesPL: 3D lateral pile-ground interaction user manual (beta 1.0), in: Department of Structural Engineering, vol. 147, University of California, San Diego, 2011.
[34] F. Paolacci, R. Giannini, P.H. Nam, D. Corritore, G. Quinci, Scores: an algorithm for records selection to employ in seismic risk and resilience analysis, Procedia Struct. Integr. 44 (2023) 307–314.
[35] V.T. Tan, N.T. Hieu, Probabilistic Seismic Hazard Assessment for Da Nang City, Vietnam, 2022.
[36] M.J.N. Priestley, G.M. Calvi, M.J. Kowalsky, Direct displacement-based seismic design of structures, NZSEE confer. 30 (2007) 1–23. Citeseer.
[37] Improvement of nonlinear static seismic analysis procedures, F. 440, FEMA, 2005.
[38] M. M, S. Marelli, B. Sudret, Uqlab User Manual – the UQLINK Module, Report UQLab-V2.1-110," Chair Ofrisk, Safety and Uncertainty Quantification, ETH Zurich, Switzerland, 2024.
[39] N.L. Da Costa, M.D. de Lima, R. Barbosa, Evaluation of feature selection methods based on artificial neural network weights, Expert Syst. Appl. 168 (2021) 114312.
[40] J.W. Baker, Efficient analytical fragility function fitting using dynamic structural analysis, Earthq. Spectra 31 (1) (2015) 579–599.